Journal of Applied Fluid Mechanics, Vol. 16, No. 7, pp. 1483-1498, 2023.
Available online at www.jafmonline.net, ISSN 1735-3572, EISSN 1735-3645.
https://doi.org/10.47176/jafm.16.07.1514

Effect of Volute-Tongue Clearance on the Aerodynamic Performance and Noise of Multi-Wing Centrifugal Fan for Air Conditioning

Y. Wei[1], L. Li[1], Y. Lun[1,2], Z. Wang[1], H. Yang[1†] and W. Zhang[1]

[1]*Key Laboratory of Fluid Transmission Technology of Zhejiang Province, Zhejiang Sci-Tech University, Hangzhou, Zhejiang 310018, China*

[2]*Hangzhou Hangyang Turbo Machinery Co., Ltd., Hangzhou, China*

†*Corresponding Author Email: yanghui@zstu.edu.cn*

(Received August 13, 2022; accepted March 26, 2023)

ABSTRACT

Multi-wing centrifugal fans are wildly used in the central air-conditioning. The influence of dimensionless clearance of the volute-tongue on aerodynamic performance and noise is studied by numerical simulation and experimental tests in this paper. The complicated internal flow related to unsteady flow in a centrifugal fan with multiple wings is investigated by numerical simulation. Besides, the influence of circumstance on the noise is analyzed. It is testified that the internal flow of centrifugal fans is ameliorated using appropriate volute tongue clearance. Reduced eddy current decreased the local-flow loss near the volute tongue and exit. The experimental results show that the static pressure of model $\triangle t/R_2$=0.12 rose to 7.5 Pa and the aerodynamics noise value reduced to 4 dB compared with that of a reference model. Meanwhile, an obvious reduction of aerodynamics noise by 3.74 dB is obtained for model $\triangle t/R_2$=0.12 installed in the air conditioning unit. The static pressure of centrifugal fan is significantly improved for the model with a cochlear tongue clearance ratio of $\triangle t/R_2$=0.12. It is further demonstrated that the proper dimensionless distance effectively suppresses the aerodynamic noise of forward multi-wing fans.

Keywords: Centrifugal fan with multi-wing; Aerodynamic noise; Interior flow; Local-flow loss; Static pressure.

NOMENCLATURE

C_ε	constant number	V	volum of computational element
C_s	Smagor constant	S_{ij}	tensor spin
D	field of flow area	T	torque
d	distance of the wall	t	time
G	filter size	T_{ij}	tensor of Lighthill
G_b	buoyancy kinetic energy	Z	blade number
G_k	turbulent kinetic energy	Δ	the filter size
K	Karman constant	ε	dissipation rate
L_p	sound level	ρ	fluid density
N	speed of the rotating impeller	η	efficiency of fan
P	pressure	Ω	flow vorticity
P_1	input power	α	Prandtl number
P_2	output power	τ_{ij}	subgrid tension
P_{ij}	stress tensor	μ_ε	viscosity coefficient
Q	value of flow	μ	coefficieent of molecular
u_t	subgrid of filtration	μ_t	coefficieent of eddy viscous

1. INTRODUCTION

The centrifugal fan is extensively applied to various industrial sectors and even has become an indispensable role in people's lives. In the past decades, many numerical simulations and experimental tests have been dedicated to the optimization and prediction of aerodynamic performance and noise (Conway *et al*. 2001; Lee *et al*. 2004; Younsi *et al*. 2007; Velarde *et al*. 2008; Heo *et al*. 2011; Hayashi and Kaneko 2014; Li *et al.* 2011). Heo *et al*. (2011) modified the trailing edge line of centrifugal -fan blades to tilt the "S" type and found that the turbulent kinetic energy of centrifugal fans decreases by comparing the original centrifugal fan. By installing the test measurements in the household refrigerator, the total noise reduction is about 2.2dB. Younsi *et al.* (2007) investigated the effects of the rotating blade, volute interior, and flow instability on the aero-acoustic characteristics of the fan using computational fluid dynamics (CFD). Tajadura *et al*. (2006) studied the numerical results with the experimental results of centrifugal fans, finding that there is a close relationship between the far-field noise signal and the pulsation of wall pressure. Liu *et al*. (2007) studied industrial centrifugal fans by the numerical method. Unsteady calculation and noise simulation are carried out for the whole volute-impeller structure (Younsi *et al.* 2007; Pavesi *et al*. 2008). The multi-wing fan, belonging to centrifugal fans, is widely used in the central air-conditioning industry (Khelladi *et al.* 2008). In general, researchers try to control the unsteady flow (Kolmogorov 1991; Sipp and Jacquin 2008; Lee *et al*. 2004; Kolář and Šístek 2015; Lun *et al*. 2019a) and suppress the aerodynamic noise by modifying the volute tongue of centrifugal fans (Bayomia *et al.* 2006; Darvish *et al*. 2015; Mao *et al.* 2018; Kim *et al.* 2019; Yang *et al.* 2019).

With the rapid development of the domestic air conditioning industry and increasing demands for this product, the miniaturization, low noise and high efficiency of air conditioning fans have been required, and the key factor affecting air conditioning noise is the multi-wing centrifugal fan. Therefore, it is an urgent problem to enhance the performance and reduce the aerodynamic noise of multi-wing centrifugal fans (Lee *et al.* 2004; Lun *et al.* 2019b). However, the problems still need to be solved, e.g., the tip-clearance flows induced by the interaction between impeller and volute -tongue dominates the performance and noise of centrifugal fans (Lun *et al.* 2019b; Kolář and Šístek 2015).

Given the above discussions, controlling the tip-clearance flows induced by the interaction between the volute tongue and impeller of centrifugal fans is essential to improve the performance of centrifugal fans and reduce aerodynamic noise.

The work focused on the effect of clearance on the internal complex unsteady characteristics, the static-pressure efficiency, and the aerodynamic noise of centrifugal fans. The main purpose was to obtain the optimal dimensionless clearance of the volute tongue by the numerical simulations of internal flow and fan performance and the noise tests. The optimal tip-clearance of volute-tongue is obtained, which can significantly improve the centrifugal-fan performance for energy saving and reduce aerodynamic noise for environmental protection.

The work mainly inquired how the tongue structure of centrifugal fans affected its performance and aerodynamic noise based on steady and unsteady simulations and experimental verification. The unsteady characteristics and aerodynamics noise are predicted utilizing CFD, and then the professional testing equipment is applied to validate the reliability of numerical results.

2. PARAMETER OF CENTRIFUGAL FANS

This section presents some primarily produced parameters and structure of the original and modified centrifugal fan, respectively.

2.1 Original Centrifugal Fans

The unsteady numerical results and experimental study on aerodynamic performance and noise are performed on a multi-wing centrifugal fan for air conditioning with 40 forwarding wing blades. Fig. 1 describes the structure of the model. An impeller, an exit, a volute, and double entrances form in the centrifugal fan. The design flow rate condition (Q_n) is 321.6m^3/h for the centrifugal fan in the work. The geometric parameters of the multi-wing centrifugal fan are shown in Table 1. Some important parameters of the original model are obtained.

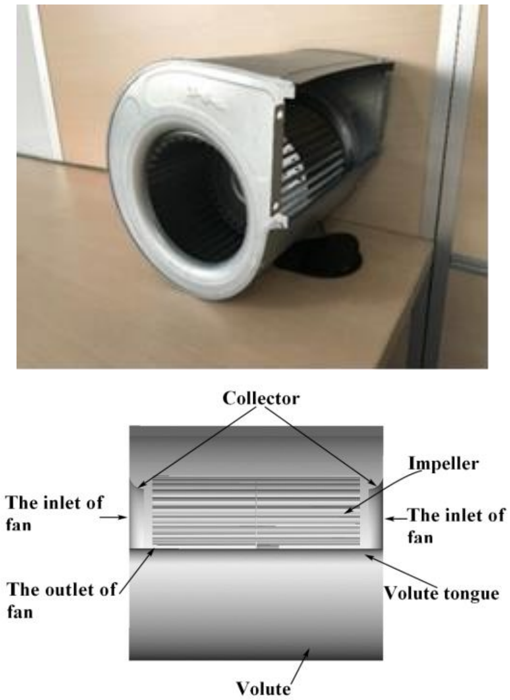

Fig. 1. Centrifugal-fan model.

Table 1 Parameters of the multi-wing centrifugal fan

Parameter	Value
Inner diameter of the impeller (D_1)	131.6 mm
Outer diameter of the impeller (D_2)	150 mm
Width of the impeller (b)	186 mm
Arc-radius of the blade (R_k)	8.95 mm
Thickness of the blade (δ)	0.45 mm
The width of the volute (B)	227.5 mm
Clearance ratio of the volute tongue ($\triangle t/R_2$、R_2—the outer radius of the impeller)	11.26 mm
Inlet angle of the blade (β_{1A})	84.83°
Outlet angle of the blade (β_{2A})	152.04°
Blade number (Z)	40

2.2 Modified Centrifugal Fan

The rotating airflow with uneven velocity and pressure distribution at outlet of impeller produces aerodynamic noise when the volute-tongue works. The clearance between impeller and volute-tongue plays an important part in improving aerodynamic performance and suppressing noise of the fan. Thus, the appropriate volute-tongue clearance of the centrifugal fun without affecting the aerodynamic can suppress the rotating noise performance of the centrifugal fun.

Figure 2 describes the clearance of volute-tongue, which is used to investigate the effect of clearance on aerodynamic performance and aerodynamic noise of the multi-wing centrifugal fan. In the work, the optimal clearance between volute-tongue and impeller is presented to enhance the performance of the multi-blade centrifugal fan and suppress the noise.

3. Numerical Methods and Experimental Programme

3.1 Numerical Setup

The internal flow of the fan is studied by numerical simulations. The impeller of the centrifugal fan is a rotating region, and the internal turbulence process is relatively complex. In general, the turbulence model of Renormalization Group (RNG) k-ε and the function of the standard wall are performed for steady simulation (Darvish *et al.* 2014). The large eddy simulation (LES) is implemented for the unsteady flow of the centrifugal fan based on the steady flow to capture the internal complex flow of the centrifugal fan (Lee *et al.* 2004). Then the aerodynamic noise is calculated based on Ffowcs Williams & Hawkings (FW-H).

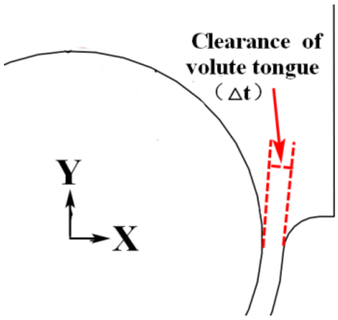

Fig. 2. Volute-tongue clearance.

3.2 Fluid-Dynamics Equations

3.2.1 Steady flow

The internal flow of the fan is performed in terms of RNG k-ε turbulence, and the governing equations are Navier-Stokes(N-S) equations (Hayashi and Kaneko 2014). The fluid-dynamics equations of the centrifugal fan are defined as

$$\frac{\partial(\rho u_i)}{\partial x_i}=0 \tag{1}$$

$$\frac{\partial(\rho u_j u_i)}{\partial x_j}=f_i-\frac{\partial P^*}{\partial x_i}+\frac{\partial\left[\mu_e\left(\frac{\partial u_i}{\partial x_j}+\frac{\partial u_j}{\partial x_i}\right)\right]}{\partial x_j} \tag{2}$$

in which ρ denotes the density of air, f_i is the component of volume force, μ_ε is the viscosity coefficient. $\mu_\varepsilon=\mu+\mu_t$, where μ is the coefficient of molecular and μ_t the coefficient of eddy viscous.

$$\mu_t=\rho C_\mu\frac{k^2}{\varepsilon}\,(C_\mu\text{=0.0845}) \tag{3}$$

The turbulent energy equation and the diffusion equation of the RNG k-ε turbulence model are used as follows.

$$\frac{\partial}{\partial t}(\rho k)+\frac{\partial}{\partial x_i}(\rho k u_i)_k=\frac{\partial}{\partial x_j}\left(\alpha_k\mu_{eff}\frac{\partial k}{\partial x_j}\right) +G_k+G_b-\rho\varepsilon-Y_M+S_k \tag{4}$$

$$\frac{\partial}{\partial t}(\rho\varepsilon)+\frac{\partial}{\partial x_i}(\rho\varepsilon u_i)=\frac{\partial}{\partial x_j}\left(\alpha_\varepsilon\mu_{eff}\frac{\partial\varepsilon}{\partial x_j}\right)+ C_{1\varepsilon}\frac{\varepsilon}{k}(G_k+G_{3\varepsilon}G_b)-C_{2\varepsilon}\rho\frac{\varepsilon^2}{k}-R_\varepsilon+S_\varepsilon \tag{5}$$

where G_k is the energy of turbulence; G_b is the energy of turbulence by buoyancy; $C_{1\varepsilon}$, $C_{2\varepsilon}$, and $C_{3\varepsilon}$ are the constant numbers; α_k and α_ε the Prandtl numbers, respectively; S_ε and S_k are given in previous work (Sipp and Jacquin 2008).

3.2.2 Transient Simulation Method

The large-eddy simulation (LES) is implemented to simulate various eddies. The average flow is greatly influenced by the large-size vortex, while the small-size vortex is dissipated in the turbulent flow (Lee *et al.* 2010). The large-scale vortex dominates in the mainstream energy, and the small-scale vortex is filtered in the LES. The former can be directly stimulated by the *N-S* equation, while the latter is solved to establish the relationship through the subgrid-scale model. Filtered variable is expressed as

$$\bar{\phi}(X)=\int_D \phi(X')G(X,X')dX' \tag{6}$$

where *D* denotes the field of flow area; *G* determins the filter size. The function of filtration is

$$\bar{\phi}(X)=\frac{1}{V}\int_V \phi(X')dX' \tag{7}$$

where *V* is the computational volume. *G(X,X')* is

$$G(X,X')=\begin{cases}\frac{1}{V}, X'\in v\\ 0, otherwise\end{cases} \tag{8}$$

The incompressible flow N-S equations are expressed as

$$\frac{\partial\rho}{\partial t}+\frac{\partial}{\partial x_i}\left(\rho\bar{u}_i\right)=0 \tag{9}$$

and

$$\frac{\partial}{\partial t}\left(\rho\bar{u}_i\right)+\frac{\partial}{\partial x_j}\left(\rho\bar{u}_i\bar{u}_j\right)=\frac{\partial}{\partial x_j}\left(\mu\frac{\partial\bar{u}_i}{\partial x_j}\right)-\frac{\partial\bar{p}}{\partial x_i}-\frac{\partial\tau_{ij}}{\partial x_j} \tag{10}$$

where τ_{ij} is the subgrid tension, denoted as

$$\tau_{ij}=\rho\overline{u_i u_j}-\rho\bar{u}_i\bar{u}_j \tag{11}$$

If the tension of the subgrid is obtained by the filtration, the eddy-viscosity equation is

$$\tau_{ij}-\frac{1}{3}\tau_{kk}\delta_{ij}=-2\mu_t\bar{S}_{ij} \tag{12}$$

where u_t denotes the turbulent viscous force of subgrid, and $\bar{S}_{ij}$ the tensor spin

$$\bar{S}_{ij}=\frac{1}{2}\left(\frac{\partial\bar{u}_i}{\partial x_j}+\frac{\partial\bar{u}_j}{\partial x_i}\right) \tag{13}$$

where μ_t can be obtained by the Samagorin-Lilly model (Sipp and Jacquin 2008), expression as

$$\mu_t=\rho L_s^2\left|\bar{S}\right| \tag{14}$$

Where

$$\left|\bar{S}\right|\equiv\sqrt{2\bar{S}_{ij}\bar{S}_{ij}} \tag{15}$$

C_S is the samagor constant, and L_s is the length of grid hybrid, defined as

$$L_s=\min\left(\kappa d, C_s V^{1/3}\right) \tag{16}$$

where κ denotes the number of von Karman, *V* is the computational element volume, *d* denotes the distance of the wall, and *Cs*=0.1 is implemented in the work.

3.2.3 Acoustic Theory

Based on the FW-H equation, the most commonly used sound-compared method of Lighthill can be implemented to solve the noises generated by different noise sources (monopole, dipole, and quadrupole), (Darvish *et al*. 2014; Mao *et al*. 2018). By specifying the location of the noise source, the time-domain integral method is adopted to solve the noise, i.e., the sound pressure value and the noise signal change with time. The time-accurate solutions can be obtained from the unsteady RANS equations, detached eddy simulation (DES), and LES equations, and the precise vortex shedding and other flow phenomena can be derived (Xu *et al.* 2018).

$$\left(\frac{1}{c^2}\frac{\partial^2}{\partial t^2}-\frac{\partial^2}{\partial x_i^2}\right)p'(x_i,t)=\frac{\bar{\partial}}{\partial t}\left\{\left[\rho_0 v_n+\rho(u_n-v_n)\right]\delta(f)\right\}-\frac{\bar{\partial}}{\partial x_i}\left\{\left[-p'_{ij}\cdot n_j+\rho u_i(u_n-v_n)\right]\delta(f)\right\}+\frac{\bar{\partial}^2}{\partial x_i x_j}\left[T_{ij}H(f)\right] \tag{17}$$

where $\frac{1}{c^2}\frac{\partial^2}{\partial t^2}-\frac{\partial^2}{\partial x_i^2}$ is the wave factor; $p'(x_i,t)$ the sound-pressure intensity at point x_i at time t; ρ, u_i, and p'_{ij} are the density, velocity, and stress tensor, respectively. $T_{ij}=-p'_{ij}+\rho u_i u_j-c^2\rho'\delta_{ij}$ is a tensor of Lighthill.

The working conditions of the numerical simulation are computed based on the experimental data. The computational boundary conditions define the inlet

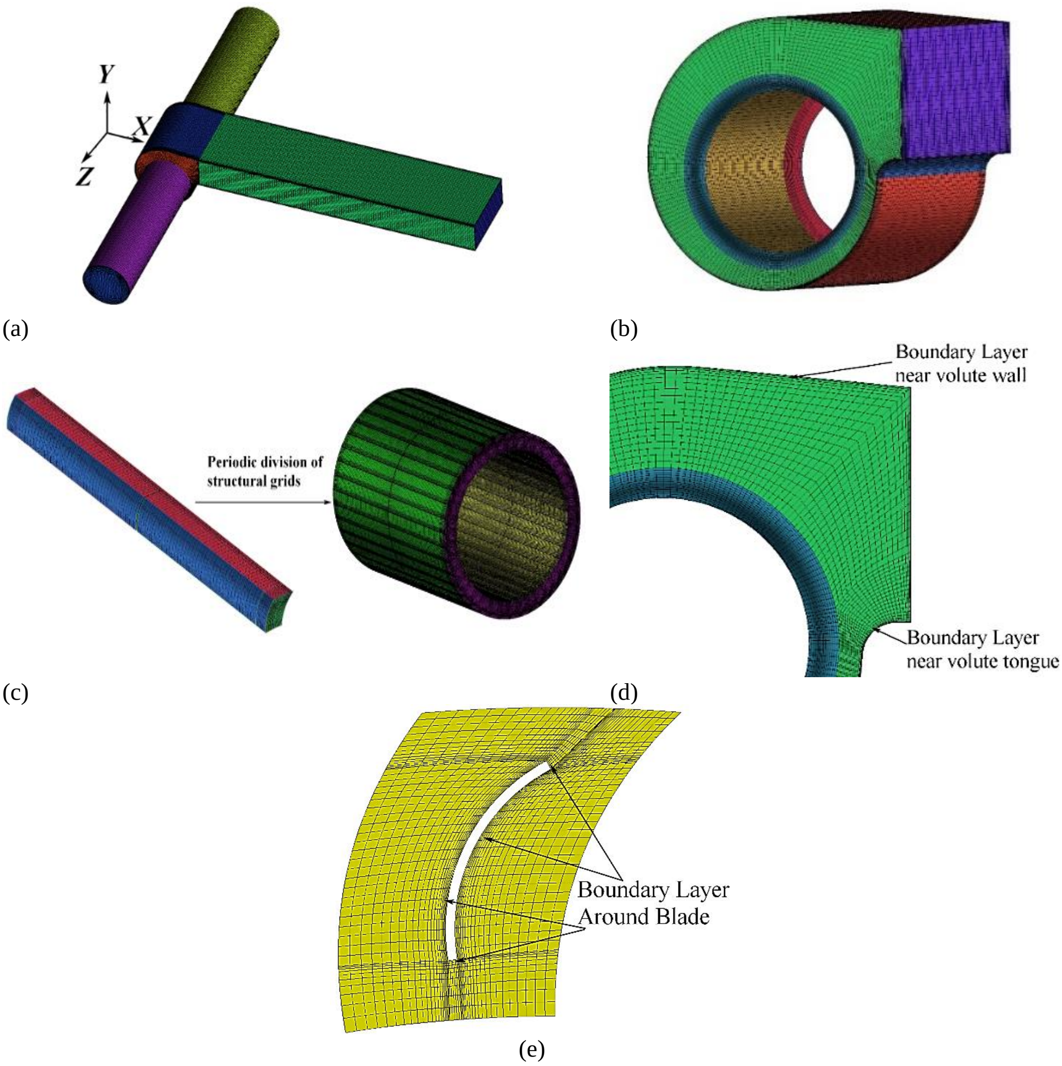

Fig. 3. Grid structure.

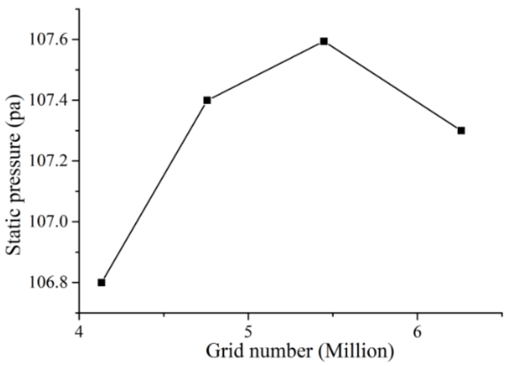

Fig. 4. Static pressure at different grid numbers.

boundary of the mass flow inlet is implemented. Meanwhile, the outlet boundary of pressure outlet boundary is used in all numerical simulations. Since the computational domain is divided into the impeller dynamic domain and other static domains, the integral domain of the impeller is set as the rotation domain when the numerical calculation is carried out. The commonly used methods are SRF, MRF, and sliding mesh for setting the rotating domain. Since the noise of the fluid is closely related to fluid-pressure fluctuation, the numerical simulation needs to be steady/ unsteady.

Preliminary time-invariant simulations can be performed using the mobile reference frame model (MRF), which is also known as the frozen rotor. That is, the fluid does not rotate, but a rotating coordinate system is introduced to make the originally stationary region form relative motion. A sliding grid is set for unsteady calculations. The steady calculation of the flow field is performed, and then the large eddy simulation is performed according to the numerical results after the convergence of the results. Finally, the noise model is turned on to carry out the final noise calculation on the unsteady results.

3.3 Mesh (Gird)

In the work, the structured grids are implemented to simulate the centrifugal fan. The increasingly accurate grids are ideal for the large eddy

Table 2 Grid number of centrifugal fans in each fluid region

Region of fluid	Grid Number	Quality of the grid (Determinant 2*2*2)
Inlet(left)	265933	0.735-0.996
Inlet(right)	293210	0.655-0.997
Impeller	4168320	0.875-0.997
Volute	417540	0.612-0.999
Outlet	302621	0.95-1
Total	5447624	/

simulation of centrifugal fans (see Figs. 3 (b) and (c)). Figure 3 displays the structural grids of the impeller domain. Figure 3 (d) shows the volute and impeller grid in the Z=0.015m plane. The grid is refined near the wall, and Fig. 3 (e) shows the mesh near the volute tongue Four different grid-number models, grids of 4132564, 4756825, 5447624, and 6258357 are performed to verify the grid independence, respectively. Figure 4 displays the static pressure at

four grid numbers. The difference in the rate of the static pressure is less than 1% at four mesh numbers. The static-pressure difference can be ignored, and the numerical results are not influenced by the grid numbers. Table 2 shows the gird number of each fluid region and the total gird number.

3.4 Laboratory of the Aerodynamics Performance and Noise

Aerodynamic performance test platform and aerodynamic noise measurement test platform of all centrifugal fans are obtained in the Inc. Yilida's laboratory. The Inc. Yilida's laboratory is Certified by Air Movement and Control Association International, Inc. (AMCA), which can obtain reliable and accurate data guarantee. The standard uncertainty of the input is synthesized into the uncertainty of the output based on the uncertainty propagation rate. The inclusion factor is determined based on the probability distribution, the expanded uncertainty of the acquisition output is calculated, and the rating results are obtained according to the expanded uncertainty of the inclusion factor and output. The GB/T 2888-2008 "methods for measuring the noise of phoenix blowers and roots blowers" is adopted to measure the aerodynamic noise characteristics of fans. The SPL(SPL) is measured at each point on the surface of the noise source in the semi-anechoic chamber, and then the average SPL is obtained in this paper. Figure 5 describes the test system of the aerodynamics performance and noise for fans. The semi-muffling method is implemented in the entire test system and the transited connection of the circular pipe is adopted between the semi-muffling chamber and the joint air chamber. The whole circuit is the closed-loop structure. The test system mainly includes the internal muffler, internal heat preservation, water chiller, automatic regulating nozzle, temperature and humidity transmitter, multiple pressure transmitters, and 20-channel microphone. The test system can synchronously measure the aerodynamic performance and noise.

The performance of the fan is evaluated by the total pressure-flow rate. In general, the total pressure is the sum of dynamic and static pressures.

The performance of a fan to discharge air is the output power per unit time：

$$P_2 = \frac{PQ}{1000*3600} \tag{18}$$

in which P_2 denotes the output power. Usual the fan shaft power is also named input power, expressed as

$$P_1 = \frac{\pi Tn}{3000} \tag{19}$$

Where P_1 denotes the input power, N denotes the speed of the rotating impeller and T is the torque.

The efficiency of centrifugal fan is

$$\eta = \frac{P_1}{P_2} = \frac{PQ}{120\pi Tn} \tag{20}$$

A sound level of the average is

$$\bar{L}_p = 10\log_{10}[\frac{1}{N}\sum_{i=1}^{N}10^{0.1(L_{p1}-k_{L1})}] - K_2 - K_3 \tag{21}$$

in which L_p denotes the sound level, N is the number of the monitoring points, L_{p1} denotes the sound level of measuring at point i, K_{L1} is the correction value of the background noise at point i, K_2 is the correction value of environment, K_3 is the correction value of the ambient pressure and temperature.

The numerical simulation for the fan is carried out at seven test conditions to prove the reliability of the numerical results. The static pressure of the fan is taken as the standard, with the numerical and experimental results compared.

Figure 6 displays the static pressure comparison between numerical and experimental results. The numerical results in agreement with the trend of static pressure measured in the test. The maximum static pressure difference between experimental and numerical results is less than 10 Pa. The maximum error of static pressure is 1%, which indicates that previous numerical results fully meet the error requirements. Therefore, the numerical simulation is reliable and can be implemented to analyze the flow and aerodynamic noise characteristics.

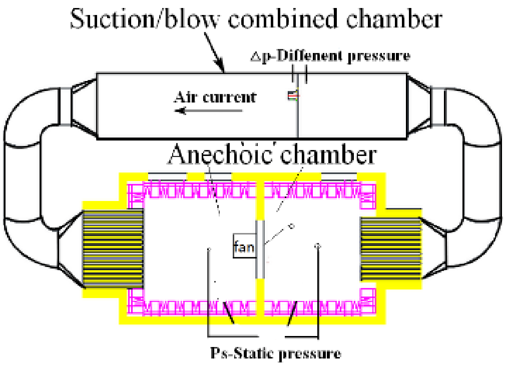

(a)

(b)

(c)

(d)

(e)

(f)

(g)

(h)

Fig. 5. Test system of the aerodynamics performance and noise for the fan.

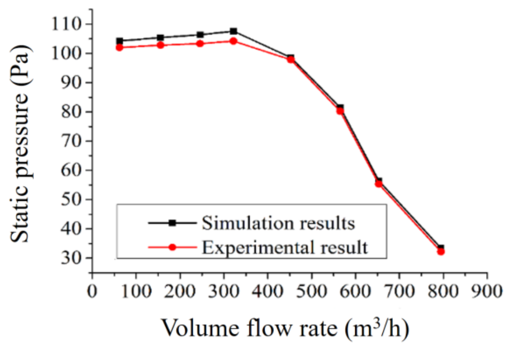

Fig. 6. Static pressure curves between numerical and experimental results.

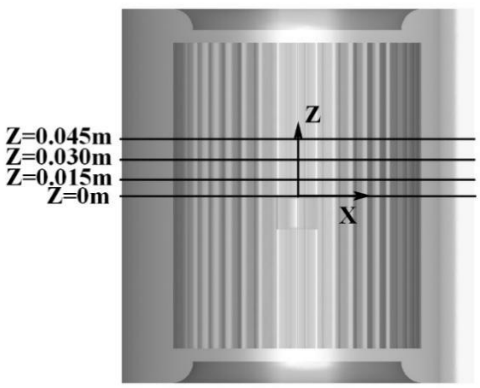

Fig. 7. Different plane positions.

4. Numerical Results and Discussions

4.1 Effect of the Clearance Between Volute and Tongue on the Internal Complex Flow

The static pressure and distribution of Q value are analyzed in this section to study the effect of different volute-tongue clearances on the internal flow of the centrifugal fan.

Figure 7 describes the different plane locations. The middle disk is plane of Z=0 mm. Three planes, Z= 0.015, 0.030, and 0.045 m, are cut along the Z-axis positive direction, respectively. The internal flow state is analyzed on three planes as follows.

In general, the largest flow loss mainly occurs in the interactive area of the impeller disc between the rotating impeller of the centrifugal fan and the volute tongue. Figure 8 illustrates the static-pressure distribution at different planes of the centrifugal fan (Z=0.015, 0.030, and 0.045 m). All the static pressure of the three models mainly occur at the position of the volute tongue on three different planes, and the static pressure value and gradient difference at the volute tongue of the reference model are greater than those of models $\triangle t/R_2$=0.12 and $\triangle t/R_2$=0.14. Interestingly, the gradient of static pressure distribution for model $\triangle t/R_2$=0.12 is the most uniform near the volute tongue compared to that of other modes, indicating that the lowest flow loss is obtained for model $\triangle t/R_2$=0.12 in the volute tongue.

The Q criterion is regarded as the physical characteristics of the local flow loss (Lee *et al*. 2004; Velarde *et al*. 2008). As a rule of vortex decision, it is used to quantitatively analyze the structure of the internal flow vortex (Lun *et al*. 2019b), expressed as

$$S_{ij} = \frac{1}{2}\left(\frac{\partial u_i}{\partial x_j} - \frac{\partial u_j}{\partial x_i}\right) \tag{22}$$

$$\Omega_{ij} = \frac{1}{2}\left(\frac{\partial u_i}{\partial x_j} + \frac{\partial u_j}{\partial x_i}\right) \tag{23}$$

$$Q = \frac{1}{2}\left(\|\Omega\|^2 - \|S\|^2\right) \tag{24}$$

$$Q = -\frac{1}{2}\left(\left(\frac{\partial u}{\partial x}\right)^2 + \left(\frac{\partial v}{\partial y}\right)^2 + \left(\frac{\partial w}{\partial z}\right)^2\right) - \frac{\partial u}{\partial y}\frac{\partial v}{\partial x} - \frac{\partial u}{\partial z}\frac{\partial w}{\partial x} - \frac{\partial v}{\partial z}\frac{\partial w}{\partial y} \tag{25}$$

where S_{ij} is the strain tensor rate, Ω_{ij} is the flow vorticity and Q is the value of Second invariant of velocity gradient tensor.

Figure 9 interprets the distribution of Q values for the centrifugal fan at different planes (*Z*=0.015, 0.030, and 0.045 m). In Fig. 9 (a), at the plane of *Z*=0.015m, a large distribution of the Q value for the reference model mainly occurs at the bottom of the volute, a high distribution of Q value for model $\triangle t/R_2$=0.12 mainly at the inlet of the impeller and a high distribution of Q value for model $\triangle t/R_2$=0.14 mainly in the impeller and volute-tongue.

For Fig. 9 (b), on the plane Z=0.030 m, a higher Q value for model $\Delta t/R2$=0.14 appears near the volute tongue, while a more uniform distribution of Q value for the reference model and model $\Delta t/R2$=0.12 appear on the whole plane. However, At the Z=0.045m plane, a smaller Q value for model $\Delta t/R2$=0.12 is less than that of the other two models near volute-tongue and at the top of volute (see Fig. 9 (c)). When the ratio of the volute tongue clearance is $\Delta t/R2$=0.12, the airflow structure is significantly improved around volute-tongue, demonstrating that the flow loss for model $\Delta t/R2$=0.12 is the lowest in the volute tongue.

4.2 Effect of Volute-Tongue Clearance on Aerodynamic Noise

The aerodynamic noise of fun is generally calculated by the FW-H equation (Darvish *et al.* 2014, Mao *et al*. 2018), which mainly forecasts the.

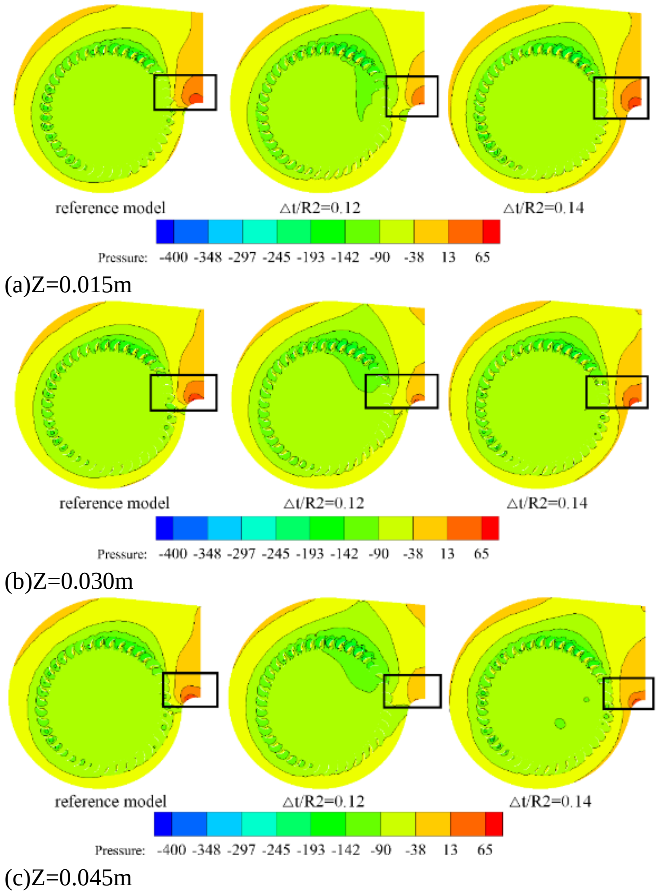

Fig. 8. Static-pressure distribution of different planes.

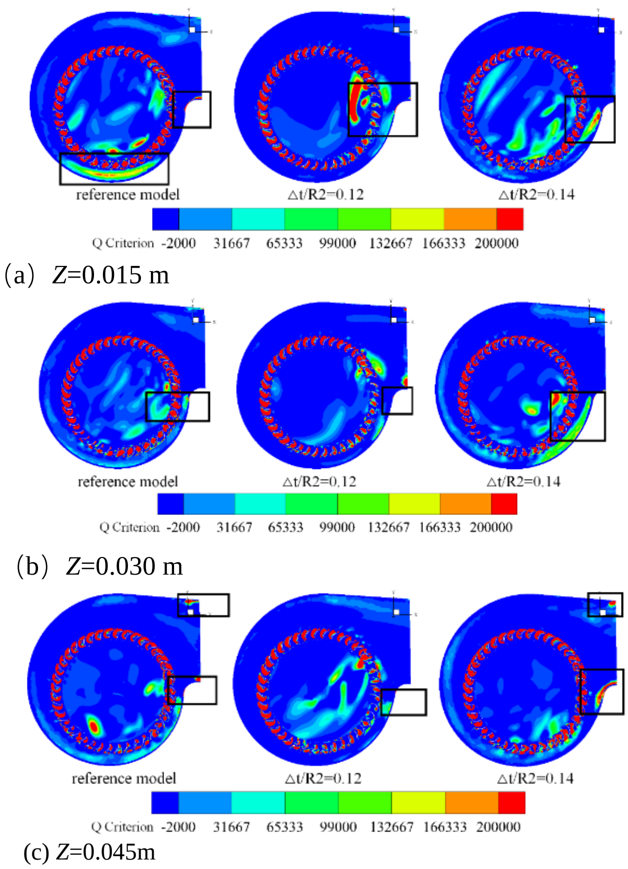

Fig. 9. Q-value distribution at different planes.

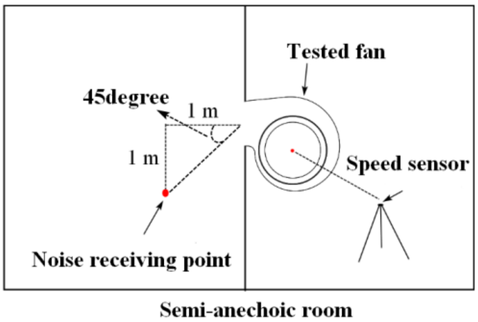

Fig. 10. Test of the centrifugal fan.

influence of volute -tongue clearance on noise of centrifugal fan in this work. The noise spectrum and 1/3 octave of the centrifugal fan are used to discuss the influence of volute-tongue clearance on noise of the fan in the following subsection

The motor separately works to determine the error before measuring the centrifugal fan. In general, the noise of the motor is much lower than that of the fan. Therefore, it does not affect the experimental results of noise. For the multi-wing fan of air conditioning, aerodynamic noise mainly comes from outlet of the fan. Figure 10 illustrates the position of the noise receiving the outlet point of the centrifugal fan. The outlet center of the volute is inclined 45° downwards, and the length is $\sqrt{2}$ meters.

The aerodynamic noise of outlet of fan is an important factor to distinguish the noise characteristics. Figure 11 shows the prediction of the noise spectrum for the fan outlet with different clearance ratios of the volute tongue and reference model at the same flow rate. It is well known that the rotating aerodynamic noise is mainly caused by the interaction between rotating blades and volute-tongue. In the first frequency (800 Hz), the SPL of blade passing frequency (BPF) for the reference model is 17 dB, 14dB for model $\triangle t/R_2$=0.12, and 16 dB for model $\triangle t/R_2$=0.14. Figure 11 shows that the discrete and broadband noises of three models. The SPL of the reference model is significantly higher than that of models $\triangle t/R_2$=0.12 and $\triangle t/R_2$=0.14, and the amplitude of reference model$\triangle t/R_2$=0.14 is slightly higher than that of model$\triangle t/R_2$=0.12. In the first frequency (800 Hz), the SPL of BPF for the reference model is 17 dB, 14dB for model$\triangle t/R_2$=0.12, and 16 dB for model $\triangle t/R_2$=0.14. The SPL increases in the base frequency with the decrease of discrete noise in the centrifugal fan.

The 1/3 octave band can distinguish the aerodynamic noise of fans (Darvish *et al.* 2014). Figure 12 illustrates the 1/3 frequency multiplication of the reference model and models $\triangle t/R_2$=0.12 and $\triangle t/R_2$=0.14 at the same speed and design flow rate. The SPL of centrifugal fan is mainly concentrated at low-frequency band with higher level. The reference model is higher than that of the other two improved models at the low-frequency band. In the ranges of 20-120 Hz, 200-400 Hz, and 500-800 Hz, the SPL of model $\triangle t/R_2$=0.12 is significantly reduced. Interestingly, a decrease of 3.8 dB for$\triangle t/R_2$=0.12 in the total SPL is obtained in our noise-predicted process.

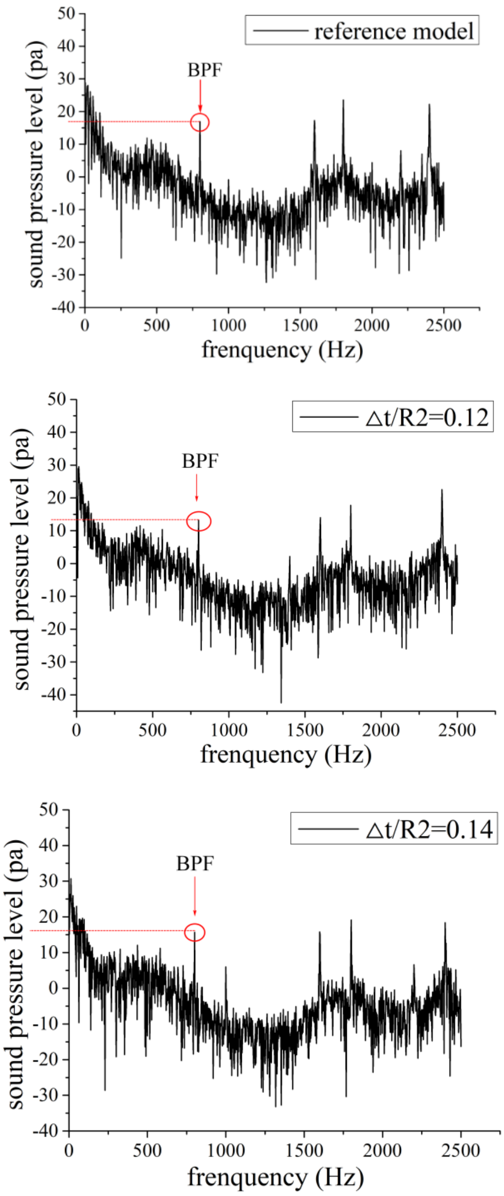

Fig. 11. Outlet-noise spectra of the centrifugal fan.

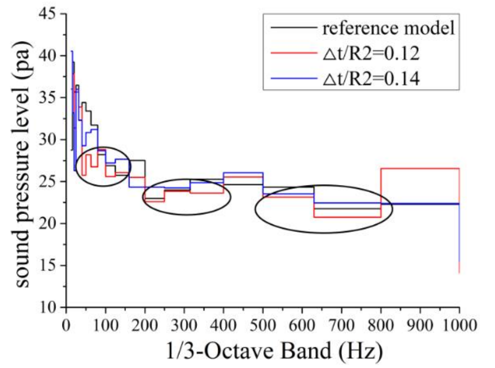

Fig. 12. 1/3 octave of the outlet noise.

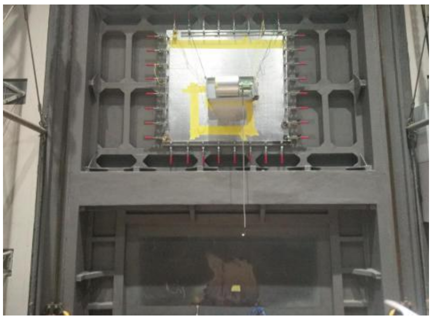

(a)

(b)

Fig. 13. Performance and noise test of the centrifugal fan in the laboratory.

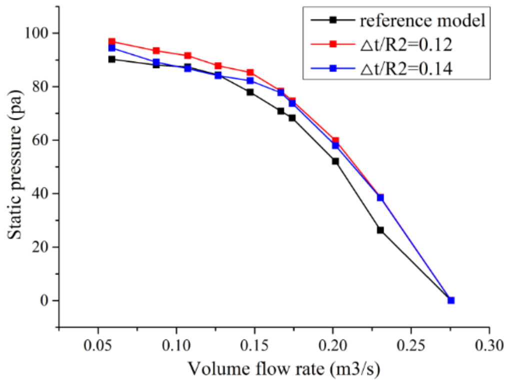

(a) Comparison of the static pressures of three models

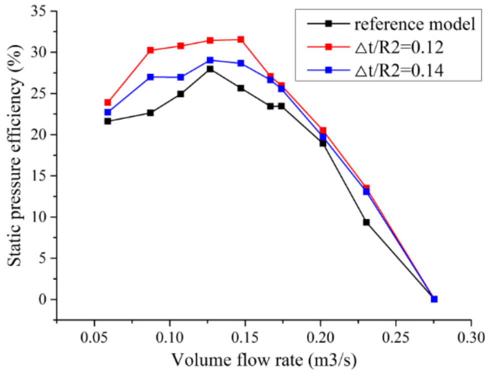

(b) Comparison of the Static-pressure efficiencies of three models

Fig. 14. Aerodynamic performance.

5. Experimental Study on Aerodynamic Performance and Aerodynamic Noise

The parameters of aerodynamic characteristics and the fan noises of a centrifugal fun with curved blades for central air conditioning are measured and collected in this section. The external characteristic curves and fan's outlet noise of the models of different volute-tongue clearance ratios at different speeds are obtained by tests in the following section.

5.1 Effect of Volute-Tongue Clearance on Aerodynamic Performance

The aerodynamic noises and performance of the reference model and models $\triangle t/R_2$=0.12 and $\triangle t/R_2$=0.14 are measured in the test system of aerodynamics performance and noise (see Fig. 13). The speed of all models is 1200 n/min. Figure 5 shows the test scheme and instruments.

Figure 14 (a) describes that static pressure of fan is gradually decreasing with increasing of flow rate. It can also obtain that static pressure of model $\triangle t/R_2$=0.12 is significantly higher than that of the reference model. The static pressure of mode $\triangle t/R_2$=0.12 rises to 3.5 Pa at the rated working condition (Q_n), and the maximum improved static pressure of mode $\triangle t/R_2$=0.12 is 7.5Pa at Q/Q_n=1.16 compared to that of the reference model. Static pressure of model $\triangle t/R_2$=0.14 rises to 4.1 Pa at a small flow rate. However, static pressure of model $\triangle t/R_2$=0.14 is almost consistent with that of the reference model at the rated condition and higher at the high flow rate. The maximum improved static pressure of mode $\triangle t/R_2$=0.14 is 6.8 Pa compared to that of the reference model.

Figure 14 (b) illustrates the comparison of static-pressure efficiencies of three models. In Fig. 13 (b), the static pressure efficiency of the centrifugal fan first increases when the flow rate is lower than the rated working condition (Q_n). However, static-pressure efficiency decreases with the increase of flow rate when the flow rate is higher than Q_n. Compared with the three models, the model $\triangle t/R_2$=0.12 is higher than that of the reference model as a whole, especially in the low flow and rated conditions, and the difference of the maximum efficiency is 3.6%. The static-pressure efficiency of reference model is lower than that of the two modified models, with a difference of maximum efficiency (3.7%). In summary, the performance of model $\triangle t/R_2$=0.12 is better than that of the reference model and model $\triangle t/R_2$=0.14.

In general, 80% of Q_n is regarded as an efficient working range. The efficient working range of the original model is the volume-flow rate from 0.1 to 0.18 (m^3/s). Figure 14 shows the comparison of the shaft powers of three models at different flow rates.

In Fig. 15, the shaft powers for mode $\triangle t/R_2$=0.12 are lower than that of mode $\triangle t/R_2$=0.14 and the

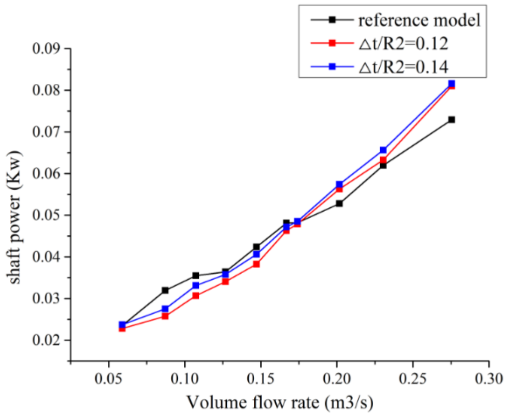

Fig. 15. Comparison of the shaft powers of three models at different flow rates.

original model in middle and high flow conditions (the efficient working range), revealing that model $\triangle t/R_2$=0.12 of the forwarding multi-wing centrifugal fan consumes less energy in the same conditions.

The laws of the fan are expressed as

$$\frac{p_2}{p_1} = \left(\frac{n_2}{n_1}\right)^2, \frac{P_2}{P_1} = \left(\frac{n_2}{n_1}\right)^3 \tag{22}$$

where P_1 and P_2 are the static pressures of fan modes 1 and 2 respectively, P_1 and P_2 the shaft powers; n_1 and n_2 the fan speeds of modes 1 and 2, respectively. According to Eq. (22), the shaft power of the centrifugal fan is greatly reduced in middle and high flow conditions. When the static pressure of the centrifugal fan of model $\triangle t/R_2$=0.12 drops to the static pressure of the reference model by reducing the speed, an increasing energy saving is realized.

5.2 Effect of Volute-Tongue Clearance on Aerodynamic Noise

The aerodynamic noises of fans are divided into the rotating noise and vortex noise (Darvish *et al*. 2014). In general, the rotating noise is formed when the working wheel rotates. The blades on the wheel hit the surrounding gas medium, causing the pressure fluctuation of the surrounding gas. For a given particle in space, whenever the blade passes, the pressure of the gas striking the particle rises and falls rapidly. The rotating blades continuously sweep one by one, which continuously produces pressure pulsation and results in great uneven airflow. Thus, the noise is radiated to the surrounding area, which is well related to the speed and number of blades (Kolář and Šístek 2015).

$$f = \frac{nzi}{60}, Hz \tag{23}$$

where n is the rotation speed of impeller, z is the number of blades and i is the wave number.

The vortex noise known as the turbulent noise is mainly brought by the boundary layer and separated vortex when the airflow flows through the blade interface, which causes pressure fluctuation on the blade and radiates an unsteady flow noise (Darvish *et al*. 2014).

All aerodynamic noises of centrifugal fans are implemented in the test system of the aerodynamics performance and noise for centrifugal fans (see Fig. 5). By receiving the noise signal from all the noise sources of the centrifugal fun, 1/3 octave plots of the three models are obtained at three different flow rates. The t rotational speed of the centrifugal fans in the test is 1,200 rpm. In general, the aerodynamic noise in 1,000-2,000 Hz is very sensitive for human ears (Darvish *et al*. 2014).

Figure 16 exhibits the comparison of 1/3 octaves of three models at different flow rates. Several well-defined peaks of the sound-pressure level are presented at 800, 1600, and 2,000 Hz and are extended over wider frequency bands. At different flow rates, the SPLs of models $\triangle t/R_2$=0.12 and $\triangle t/R_2$=0.14 in 1/3 octave are lower than that of the reference model in different multiple frequencies.

Meanwhile, the SPL of model $\triangle t/R_2$=0.12 model in 1/3 octave is also lower than that of model $\triangle t/R_2$=0.14 at different multiple frequencies. Thus, when the dimensionless volute tongue clearance ($\triangle t/R_2$) is equal to 0.12 in the present parameters of the forwarding centrifugal fan, the aerodynamic noise is reduced at different flow rates. The increased clearance of the cochlear tongue is one of the measures to control the noise of the fan. The improved cochlear tongue needs to ensure that the aerodynamic performance is not reduced, with the noise is considered. Therefore, the reasonable clearance ratio of the cochlear tongue is important for the aerodynamic performance and noise.

A-weighted sound pressure is studied in a wide range of flow rates by the experimental measurement to further reveal the effect of the dimensionless volute tongue clearance on the aerodynamic noise. Figure 17 shows the noise values of the three models at ten flow rates. At different flow rates, the noise values of models $\triangle t/R_2$=0.12 and $\triangle t/R_2$=0.14 are lower than that of the original model. Compared to models $\triangle t/R_2$=0.12 and $\triangle t/R_2$=0.14, the noise value of $\triangle t/R_2$=0.14 is lower than that of $\triangle t/R_2$=0.12 at low flow rates, and the model noise value of $\triangle t/R_2$=0.12 is lower than that of $\triangle t/R_2$=0.14 at the designed flow rate and large flow rate.

Interestingly, the maximum noise of mode $\triangle t/R_2$=0.12 decreases by 4 dB at a small flow rate, which indicates that the mode of the forward multi-wing fan for the clearance ratio of $\triangle t/R_2$=0.12 greatly controls the aerodynamic noise. However, given the practical application of centrifugal fan, the general central air conditioning system runs at a flow rate of 340 m^3/h (about 0.11 m^3/h) and above, which is not enough to meet the operation demand at a small flow rate. The cochlear tongue clearance ratio of $\triangle t/R_2$=0.12 is the most effective dimensionless distance to suppress the aerodynamic noise of the forward multi-wing fan.

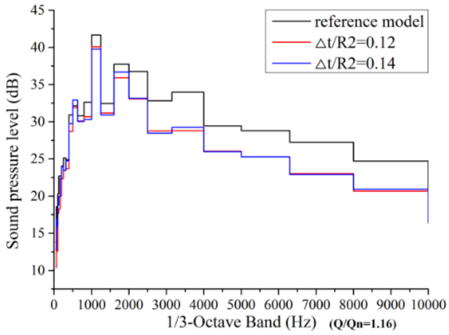

(a)Q/Q$_n$=1.16

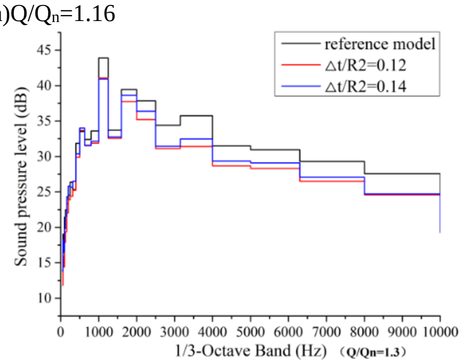

(b)Q/Q$_n$=1.3

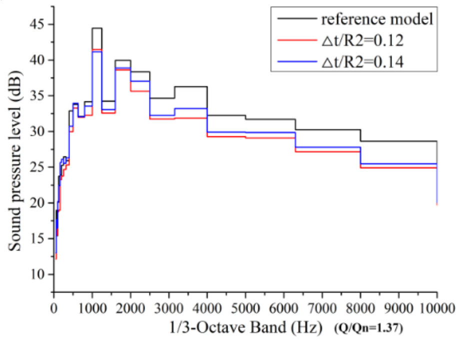

(c)Q/Q$_n$=1.37

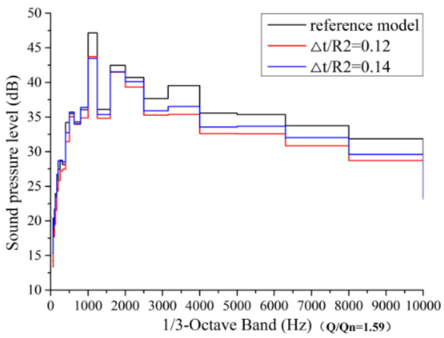

(d)Q/Q$_n$=1.59

Fig. 16. Comparison of the 1/3-Octave Band of three models at different flow rates

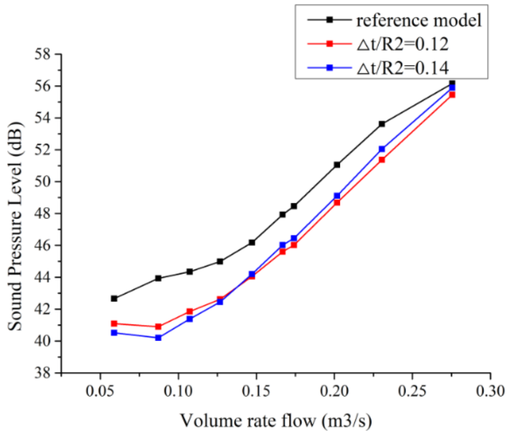

Fig. 17. Comparison of the sound-pressure levels of three models at different flow rates.

5.3 Effect of Volute-Tongue Clearance on Aerodynamic Noise

The aerodynamic noise of a single fan with different clearance ratios have been studied in detail. However, the forward centrifugal fan works in the actual unit of the wind disc, which brings some insights to the aerodynamic noise due to the change of the actual working environment. According to the actual operation of centrifugal fan, the two models are tested separately in units to verify the aerodynamic noise of model$\triangle t/R_2$=0.12 and the reference model in the test system of the aerodynamics performance and noise (see Fig. 18). In the actual working environment, the static pressures of 50, 30, and 12 Pa are generally implemented, so three different working conditions are tested to compare the aerodynamic-noise characteristics between model $\triangle t/R_2$=0.12 and the reference model in the actual unit of the wind disc. The rated flow rate for model $\triangle t/R_2$=0.12 and the reference model is 340m^3/h, and the static pressures of 50, 30, and 12 Pa of the centrifugal fan are achieved by adjusting the rotation speed in the test system. The 1/3 octave is one of the most effective method to reveal the aerodynamic noise (Kim *et al.* 2019).

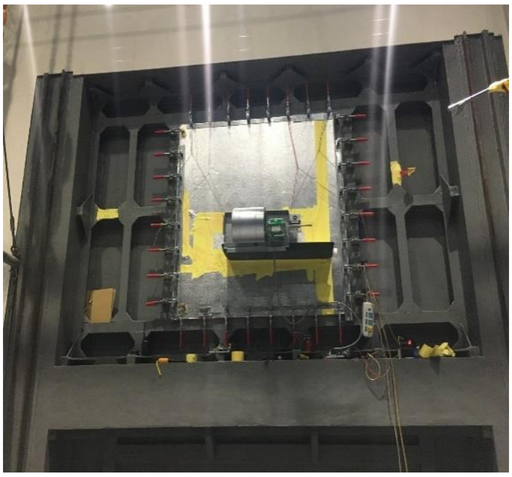

Fig. 18. Units of the centrifugal fan.

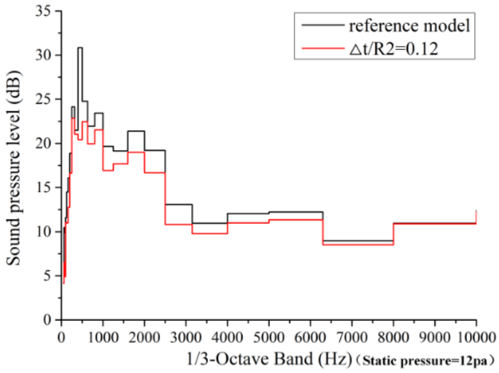

(a) Static pressure=12Pa

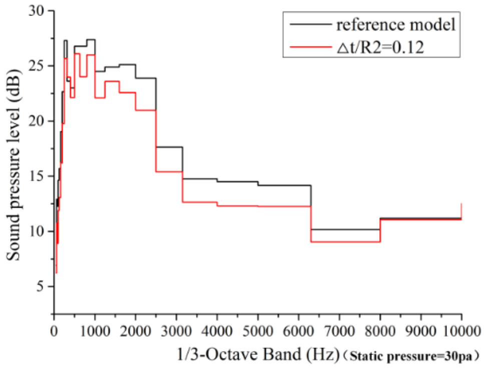

(b)Static pressure=30Pa

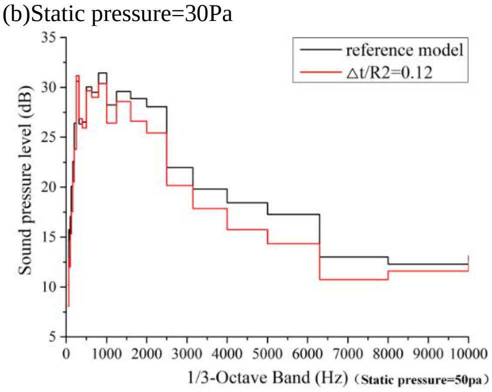

(c)Static pressure=50Pa

Fig. 19. 1/3 octave of the centrifugal fan unit.

Figure 19 shows the analysis of 1/3 octave of each unit at the different static pressures of 50, 30, and 12 Pa. The high SPL mainly occurs at 500 to 2,000 Hz. At the static pressure of 12Pa in Fig. 19 (a), the SPL of 1/3 octave of model△t/R_2=0.12 in the actual unit of the wind disc is lower than that of for the reference model, revealing that the broadband noise is controlled. Amazingly, the comparison of the SPLs between the reference model and model △t/R_2=0.12 reveals a sharp descend at 800 Hz, represented as discrete noise. Besides, the SPL gradually decreases with the increasing frequency. That of model △t/R_2=0.12 is lower than that of the reference model at different multiple frequencies. Table 3 shows the value of the SPL.

According to Table 3, comparing to the reference model at the static pressure of 50 Pa, the aerodynamic noise of model △t/R_2=0.12 in the actual unit of the wind disc is reduced by about 1

Table 3. Noise values of different units under different working conditions

	Pressure 50Pa	Pressure 30Pa	Pressure 12Pa
Reference model (Total SPL, dB)	39.81983	36.21795	34.73544
△t/R_2=0.12(Total SPL, dB)	38.87528	34.56734	31.02209

dB. The noise is reduced by about 1.7dB compared with that of the reference model at the static pressure of 30 Pa. Interestingly, at the static pressure of 12 Pa, the aerodynamic noise is reduced by about 3.7 dB compared with that of the reference model. According to the specific total SPL, the model with the volute-tongue clearance ratio of △t/R_2=0.12 is a better method to control the aerodynamic noise in the units, which realizes environmental protection by reducing the aerodynamic load of centrifugal fan.

6. Conclusions

Based on the numerical calculation and experimental research, effects of different volute-tongue clearance ratios on the performance and noise are studied in this paper. The distribution of static-pressure and Q-value near volute-tongue are analyzed. Then, the noise curve and spectrum are explained.

The local flow loss near volute-tongue and volute outlet of the centrifugal fan is controlled by the reasonable clearance ratio of the volute-tongue. The circulation of some air is prevented and complex flow structure such as eddy current with backflow reduced.

The experimental results further demonstrate that an increase of static pressure by 3.4 Pa for model△t/R_2=0.12 is obtained compared with that of the reference model at the rated working condition (Q_n). The static pressure of model △t/R_2=0.12 rose by 7.5 Pa at a flow of Q/Q_n=1.16. The maximum static pressure efficiency rose by 3.6% in the low flow and rated conditions.

The parameters of the volute tongue are related to the discrete noise of centrifugal fan. To increase the volute tongue clearance is beneficial to reduce the pressure fluctuation of the surrounding gas and aerodynamic noise. It is displayed that the noise values of two models (measured by a single machine) are lower than that of the reference model at different flow rates by the experimental results. Compared with models △t/R_2=0.12 and △t/R_2=0.14, the noise value of model △t/R_2=0.14 is lower than that of model △t/R_2=0.12 at the low flow rate. However, the model △t/R_2=0.12 has a lower noise value than model △t/R_2=0.14 at the designed flow rate and large flow rate.

The noise measurements are carried out for the units of model $\triangle t/R_2$=0.12 and the reference model according to the actual operation of the centrifugal fan in the central air conditioning system. It is obtained that that the noise is reduced by about 1dB at the static pressure of 50Pa, and the noise is reduced by about 1.7dB at a static pressure of 30 Pa. Amazingly, the noise is reduced as much as 3.7dB. Interestingly, it is further found that the dimensionless tongue-clearance ratio of $\triangle t/R_2$=0.12 suppresses the aerodynamic noise of the forward multi-wing fan realizing environmental protection and significantly improves the static pressure of the centrifugal fan that can achieve energy saving by reducing the speed of the centrifugal fan.

ACKNOWLEDGMENT

This work was supported by the National Natural Science Foundation of China (U22A20589), Natural Science Foundation Key Projects of Zhejiang Province (LZ22E060002), the Science and Technology Plan Project of Zhejiang Province (LGG21E060003, LZY22E060005, 2021C01049).

REFERENCES

Bayomia, N. N., A. A. Hafiza and A. M. Osman (2006). Effect of inlet straighteners on centrifugal fan performance. *Energy Conversion and Management* 47, 3307-3318.

Conway, S., D. Caraeni and L. Fuchs (2001). Large-eddy simulation of the flow through the blades of a swirl generator. *International Journal of Heat and Fluid Flow* 21, 664-673.

Darvish, M., B. Tietjen, D. Beck and S. Frank (2014, June). Tonal noise reduction in a radial fan with forward-curved blades. In *Proceedings of the ASME Turbo Expo 2014: Turbine Technical Conference and Exposition. Volume 1A: Aircraft Engine; Fans and Blowers,* Düsseldorf, Germany.

Darvish, M., S. Frank and C. O. Paschereit (2015). Numerical and experimental study on the tonal noise generation of a radial fan. *Journal of Turbomachinery* 137(10), 101005.

Heo, S., C. Cheong and T. H. Kim (2011). Development of low-noise centrifugal fans for a refrigerator using inclined S-shaped trailing edge. *International Journal of Refrigeration-Revue International Du Froid* 34(8), 2076-2091.

Hayashi, I. and S. Kaneko (2014). Pressure pulsations in piping system excited by a centrifugal turbomachinery taking the damping characteristics into consideration. *Journal of Fluids and Structures* (45), 216-234.

Khelladi, S., S. Kouidri, F. Bakir and R. Rey (2008). Predicting tonal noise from a high rotational speed centrifugal fan. *Journal of Sound and Vibration* 313(1-2), 113-133.

Kolmogorov, A. N (1991). The Local Structure of Turbulence in Incompressible Viscous Fluid for Very Large Reynolds Numbers. *Proceedings of the Royal Society A: Mathematical* 434(1890), 9-13.

Kim, S. J., H. J. Sung, S. Wallin and A. V. Johanssin (2019). Design of the centrifugal fan of a belt-driven starter generator with reduced flow noise. *International Journal of Heat and Fluid* 76, 72-84.

Lee, S., H. J. Kim, and A. Runchal (2004). Large-eddy simulation of unsteady flows in turbomachinery. *Proceedings of the Institution of Mechanical Engineers Part A Journal of Power & Energy* 218, 463-475.

Lun, Y. X., L. M. Lin, H. J. He, X. X. Ye, Z. C. Zhu and Y. K. Wei (2019a). Effects of vortex structure on performance characteristics of a multiblade fan with inclined tongue. *Proceedings of the Institution of Mechanical Engineers Part A Journal of Power and Energy* 233(8), 1007-1021.

Lun, Y. X., X. X. Ye, L. M. Lin, C. L. Ying and Y. K. Wei (2019b). Unsteady characteristics of forward multi-wing centrifugal fan at small flow rate. *Processes* 7(10), 691.

Liu, Q., D. Qi and H. Tang (2007). Computation of aerodynamic noise of centrifugal fan using large eddy simulation approach, acoustic analogy and vortex sound theory. *Proceedings of the Institution of Mechanical Engineers Part A-Journal of Power and Energy* 221(11), 1321-1332.

Li, C. X., S. L. Wang and Y. K. Jia (2011). The performance of a centrifugal fan with enlarged impeller. *Energy Conversion and Management* 52, (8-9), 2902-2910.

Lee, S., S. Heo and C. Cheong (2010). Prediction and reduction of internal blade-passing frequency noise of the centrifugal fan in a refrigerator. *International Journal of Refrigeration-Revue International Du Froid* 33(6), 1129-1141.

Mao, Y. J., Z. W. Hu and C. Xu and G. Ghorbaniasl (2018). Vector aeroacoustics for a uniform mean flow: acoustic velocity and vortical velocity. *AIAA Journal* 56(7), 2782-2793.

Pavesi, G., G. Cavazzini and G. Ardizzon (2008). Time-frequency characterization of the unsteady phenomena in a centrifugal pump. *International Journal of Heat Fluid Flow* 29(5), 1527-1540.

Sipp, D. and L. Jacquin (2008). *A Criterion of Centrifugal Instabilities in Rotating Systems*. Springer Berlin Heidelberg.

Tajadura, R. B., V. S. Suarez, J. P. H. Cruz and C. S. Morros (2006). Numerical calculation of pressure fluctuations in the volute of a centrifugal fan. *Journal of Fluids Engineering* 128, 359-369.

Velarde Suarez, S., R. Ballesteros Tajadura, C.

Santolaria Morros and B. Pereiras García (2008). Reduction of the aerodynamic tonal noise of a forward-curved centrifugal fan by modification of the volute tongue geometry. *Applied Acoustics* 69(3), 225-232.

Kolář, V. and J. Šístek (2015). Corotational and compressibility aspects leading to a modification of the vortex-identification Q-criterion. *AIAA Journal* 53, 2406-2410.

Xu, C., Y. J. Mao and Z. W. Hu and G. Ghorbaniasl (2018). Vector aeroacoustics for a uniform mean flow: acoustic intensity and acoustic power. *AIAA Journal* 56(7), 2794-2805.

Younsi, M., F. Bakir, S. Kouidri and R. Rey (2007). Numerical and experimental study of unsteady flow in a centrifugal fan. *Proceedings of the Institution of Mechanical Engineers Part A-Journal of Power and Energy* 221(A7), 1025-1036.

Yang, H., P. Yu, J. Xu, C. Ying and Y. Wei (2019). Experimental investigations on the performance and noise characteristics of a forward-curved fan with the stepped tongue. *Measurement & Control* 22, 1480-1488.